Target Identification from Coded Diffraction Patterns via Template Matching

Andrés Jerez[1], Samuel Pinilla[2], Hans Garcia[2], Henry Arguello[3]
[1]*Dept. of Physics*, [2]*Dept. of Electrical Engineering*, [3]*Dept. of Computer Science*
Universidad Industrial de Santander, Bucaramanga, Colombia

***Abstract*—Traditional target detection techniques have been developed using measurements from the object acquired by optical systems that are only able to measure its intensity, losing its optical phase information. The optical phase, for instance, allows describing the shape and depth of an object. This work proposes a target identification methodology that operates over measurements acquired through an optical system that collects coded diffraction patterns (CDP). In contrast to traditional detection techniques, the proposed methodology is able to incorporate the optical phase information of an object as a discriminant in the target detection task. The proposed methodology consists of two steps: first, an estimation of the scene from the acquired CDP is accomplished, second, a scanning procedure with a reference pattern over the estimated scene is performed. Numerical results show that the phase information can be used as an identification discriminant for target detection. Also, simulations demonstrate that the proposed methodology is able to identify a target under highly noisy scenarios using one single snapshot with a success rate up of 84%. Furthermore, it is worth to mention that to the best of our knowledge this is the first methodology that uses the optical phase of an object as a target identification discriminant.**

I. Introduction

Target identification is a task that allows the detection of an object of interest in a scene. This task has been studied in several areas such as astronomy [1], medicine [2], and robotics [3], among others. The target identification can be performed through a commonly used technique called template matching (TM) [4]. Specifically, TM allows the target identification using correlation analysis, which consists on scanning a scene pixel by pixel using a reference pattern, to calculate a numerical index that represents the similarity between the scene and the reference pattern. TM has been also studied by including a circular harmonic filter (CHF) correlation, which is invariant to different geometrical and noisy factors [5], [6].

Traditionally, target identification techniques have been applied using measurements from the scene acquired through optical systems that can only capture its intensity, losing the optical phase information. Notice that the optical phase is able to describe the shape and depth of an object, which cannot be discriminated by just the intensity data [7]. In this regard, the estimation of the optical phase of a scene from phaseless measurements is called the phase retrieval (PR) problem [8]. Several algorithms have been developed to estimate the optical phase in a scene from measurements that are acquired under a setup that collects coded diffraction patterns (CDP) [9]. From the state-of-the-art is known that designing an initialization strategy to solve the PR problem is critical to accurately recover the image using less computational time and measurements. Recently, several methods [10]–[12] have been developed to initialize this problem even exploiting prior information of the image of interest such as sparsity. For instance, in [10] an orthogonal-promoting initialization (OPI) is presented to estimate the scene of interest considering the largest eigenvector and the power iteration method. However, the literature of PR has not reported studies on how to detect or identify an object from CDP using its optical phase as an identification discriminant.

This work proposes a target identification methodology based on TM that is able to incorporate the optical phase of an object as an identification discriminant. Since no explicit target identification approaches that include the optical phase as discriminant variable exists in the literature, we consider a methodology that operates over measurements acquired from an optical system that records CDP, consisting of two steps: first, an estimation of the scene is performed, second, a scanning procedure using a reference pattern over the estimated scene is accomplished. Specifically, for the first step, we propose an initialization procedure based on OPI to estimate the scene. Also, we use TM as the identification methodology since it involves the fast Fourier transform to calculate the similarity indices [4]. Simulation results show that the proposed identification methodology is able to use the phase information as an identification discriminant for target detection tasks. In particular, the proposed methodology can detect a target even in highly noisy scenarios with a success rate of up 84% using one single snapshot. Also, from the numerical results, it can be concluded that the proposed initialization procedure requires less number of phaseless measurements to better estimate the scene compared to state-of-the-art initialization procedures.

Notation. We denote $(\cdot)^T$, $\overline{(\cdot)}$, and $(\cdot)^H$ as the matrix transpose, conjugate, and conjugate transpose operations, respectively. Additionally, $\mathcal{F}(\cdot)$ and $\mathcal{F}^{-1}(\cdot)$ represent the two-dimensional Fourier and inverse Fourier transform, respectively. The operator $\circ$ corresponds to the Hadamard product. The floor operation $\lfloor\cdot\rfloor$ returns the greater integer, smaller than or equal to the given number. For vectors $\|\mathbf{x}\|_p$ is the usual ℓ_p norm. Also, $(\mathbf{w})_i$ denotes the i-th entry of vector $\mathbf{w}$. For matrices the (a,b)-th entry of $\mathbf{W}$ is denoted by $(\mathbf{W})_{a,b}$. Finally, the distance between two complex vectors $\mathbf{w}_1$, $\mathbf{w}_2$ $\in \mathbb{C}^n$ is given by

$$\operatorname{dist}(\mathbf{w}_1,\mathbf{w}_2) = \min_{\theta\in[0,2\pi)} \|\mathbf{w}_1 e^{-j\theta} - \mathbf{w}_2\|_2, \tag{1}$$

where $j=\sqrt{-1}$.

978-9-0827-9703-9/19/$31.00 ©2019 IEEE

II. Acquisition System

This section introduces an optical system that collects CDP of a scene, which is illustrated in Fig. 1. Further, in contrast with state-of-the-art optical setups used for target identification, this architecture allows the optical phase estimation of an object from the acquired CDP [13].

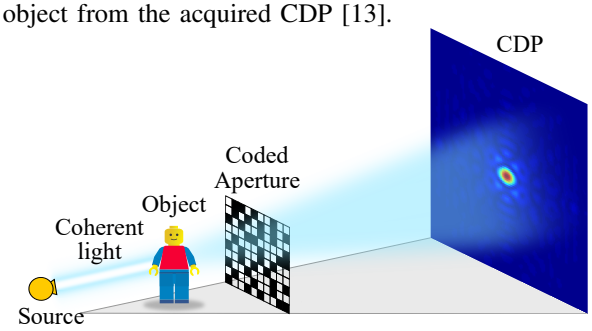

Fig. 1: Schematic representation of a system that acquires CDP.

Notice that Fig. 1 includes a coded aperture between the object of interest and the sensor. Specifically, this optical element modulates the signal before being finally measured at the sensor. In fact, if we change the spatial configuration of the coded aperture, this acquisition system allows capturing multiple snapshots of the scene. Mathematically, the acquisition process of CDP through the system illustrated in Fig. 1 is given by

$$\mathbf{y}_\ell = \left|\mathbf{F}\mathbf{D}_\ell\mathbf{x}\right|^2, \ell = 1, \cdots, L, \tag{2}$$

where $\mathbf{y}_\ell \in \mathbb{R}^n$ represents the acquired measurements at each snapshot indexed by ℓ, $\mathbf{F} \in \mathbb{C}^{n\times n}$ corresponds to the Fourier discrete transformation matrix, $\mathbf{D}_\ell \in \mathbb{C}^{n\times n}$ is a diagonal matrix that represents the coded aperture at each snapshot ℓ, $\mathbf{x} \in \mathbb{C}^n$ is the desired unknown object and $|\cdot|$ represents the pointwise magnitude. Further, defining $\mathbf{y} = [\mathbf{y}_1^T, \cdots, \mathbf{y}_L^T]^T \in \mathbb{R}^{m=nL}$ and the matrix $\mathbf{A} = [\mathbf{D}_1\mathbf{F}, \cdots, \mathbf{D}_L\mathbf{F}]^T$, we can rewrite the quadratic model in (2) as

$$\mathbf{y} = |\mathbf{A}\mathbf{x}|^2, \tag{3}$$

where each row of $\mathbf{A}$ is given by $\mathbf{a}_i = \overline{\mathbf{D}}_{r_i}\mathbf{f}_{u_i}$ with $r_i = \lfloor i/n \rfloor + 1$, $u_i = (i-1) \mod n + 1$, and $\mathbf{f}_{u_i}$ the rows of $\mathbf{F}$, for $i = 1 \cdots nL$. Also, we specify that the entries of each matrix $\mathbf{D}_\ell$ are $i.i.d.$ copies of a discrete random variable d obeying $|d| \leq 1$.

Considering the illustrated system in Fig. 1, and the acquisition model in (3), this work develops a target identification methodology from CDP that incorporates the optical phase as a discriminant. This approach will be detailed explained in Section III. Finally, it is worth to mention that in the state-of-the-art has not been previously studied how to identify an object by exploiting its optical phase by using CDP.

III. Target Identification Methodology

In this section, we describe the proposed target identification methodology, which includes two main stages: (i) an estimation of the scene from CDP based on OPI as introduced in [10], and (ii) a detection procedure that follows a TM methodology including the optical phase information.

A. Scene Estimation

Observe that the measurements in (2) can be rewritten as

$$(\mathbf{y})_i = |\langle \mathbf{a}_i, \mathbf{x}\rangle|^2, i = \{1, \cdots, m\}. \tag{4}$$

Then, taking (4) into account, define the set $I_0 \subset \{1, \cdots, nL\}$ as the collection of indices corresponding to the smallest values of $\{(\mathbf{y})_i/\|\mathbf{a}_i\|_2\}$. Thus, according to [10], OPI can be formulated as

$$\mathbf{z}_0 = \underset{\|\mathbf{z}\|_2=1}{\operatorname{argmin}} \ \mathbf{z}^H \left(\frac{1}{|I_0|}\sum_{i\in I_0}\frac{\mathbf{a}_i\mathbf{a}_i^H}{\|\mathbf{a}_i\|_2^2}\right)\mathbf{z}. \tag{5}$$

Notice that (5) implies finding the smallest eigenvalue of matrix $\frac{1}{|I_0|}\sum_{i\in I_0}\frac{\mathbf{a}_i\mathbf{a}_i^H}{\|\mathbf{a}_i\|_2^2}$, which calls for eigen-decomposition or matrix inversion, and each of these operations typically require a computational complexity $\mathcal{O}(n^3)$ [10]. However, we can avoid this step by manipulating (5) as follows

$$\sum_{i\in I_0}\frac{\mathbf{a}_i\mathbf{a}_i^H}{\|\mathbf{a}_i\|_2^2} = \sum_{i=1}^{nL}\frac{\mathbf{a}_i\mathbf{a}_i^H}{\|\mathbf{a}_i\|_2^2} - \sum_{i\in \overline{I}_0}\frac{\mathbf{a}_i\mathbf{a}_i^H}{\|\mathbf{a}_i\|_2^2}, \tag{6}$$

where $\overline{I}_0$ is the complement of I_0. Further, in order to rewrite the term $\sum_{i=1}^{nL}\frac{\mathbf{a}_i\mathbf{a}_i^H}{\|\mathbf{a}_i\|_2^2}$, we proceed as follows. Observe that

$$\|\mathbf{a}_i\|_2^2 = \sum_{p=1}^{n}\left|(\overline{\mathbf{D}}_{r_i})_{p,p}(\mathbf{f}_{u_i})_p\right|^2 = \|\mathbf{D}_{r_i}\|_F^2, \tag{7}$$

given that $\mathbf{F}$ is an orthogonal matrix. Thus, from (7) we have

$$\sum_{i=1}^{nL}\frac{\mathbf{a}_i\mathbf{a}_i^H}{\|\mathbf{a}_i\|_2^2} = \sum_{\ell=1}^{L}\frac{\mathbf{D}_\ell^H\mathbf{D}_\ell}{\|\mathbf{D}_\ell\|_F}. \tag{8}$$

Observe that, if we assume that the set of coded apertures satisfies $\sum_{\ell=1}^{L}\mathbf{D}_\ell^H\mathbf{D}_\ell = r\mathbf{I}$, from (8), it can be concluded that $\sum_{i=1}^{nL}\frac{\mathbf{a}_i\mathbf{a}_i^H}{\|\mathbf{a}_i\|_2^2} = c\mathbf{I}$ for some constant $c > 0$. Thus, considering this observation, (5) can be approximated as

$$\mathbf{z}_0 = \underset{\|\mathbf{z}\|_2=1}{\arg\max} \ \mathbf{z}^H \left(\frac{1}{|\overline{I}_0|}\sum_{i\in \overline{I}_0}\frac{\mathbf{a}_i\mathbf{a}_i^H}{\|\mathbf{a}_i\|_2^2}\right)\mathbf{z}, \tag{9}$$

which meets the numerical formulation of OPI in [10]. Further, it is important to mention that OPI was originally introduced assuming that the sampling vectors $\mathbf{a}_i$ follow a Gaussian distribution. In contrast, this work derives an initialization procedure based on OPI with the sampling vectors modeling a realistic acquisition system. Thus, considering the previous remarks, we theoretically establish in Theorem 1 that (9) can approximate the signal of interest with probability of at least $1 - \exp(-C_0 n)$.

Theorem 1. *Consider noise-free measurements* $(\mathbf{y})_i = |\langle \mathbf{a}_i, \mathbf{x}\rangle|^2$ *as defined in* (4)*, and assume that the set of coded apertures satisfies* $\sum_{\ell=1}^{L}\mathbf{D}_\ell^H\mathbf{D}_\ell = r\mathbf{I}$ *for some* $0 < r \leq L$.

Then, with probability of at least $1-\exp(-C_0 n)$ *for some constant* $C_0>0$*, the vector* $\mathbf{z}_0$ *returned by* (9) *satisfies*

$$\operatorname{dist}(\mathbf{z}_0,\mathbf{x}) \leq \rho\|\mathbf{x}\|_2, \tag{10}$$

for some constant $\rho\in(0,1)$*, provided that* $m \geq |\overline{I}_0|n$*, and for a sufficiently large* n*.*

Proof. See Appendix A. □

In order to solve (9), the Algorithm 1 presents the power iteration method. Observe that this method requires the sampling vectors and the acquired CDP. Further, following the iteration process in Algorithm 1, in line 7 the estimation of the scene is calculated. In line 8, a low pass filtering process over $\tilde{\mathbf{z}}^{(t+1)}$ is accomplished. The motivation for this step comes from the fact a scene mostly contains low frequencies [14]. Specifically, this characteristic can be exploited by suppressing the high frequencies, in this case, by the low pass filter $\mathcal{G}$. In particular, for this work, $\mathcal{G}$ was fixed as the Gaussian filter. It is worth to stress here that the main differences of the proposed initialization respect to OPI are the inclusion of the filtering step, and the theoretical extension to CDP. In fact, Section IV will numerically show that performing the filtering step is crucial to better estimate the scene with a fewer number of phaseless measurements. Finally, Algorithm 1 returns the scaled vector $\mathbf{z}_0$ as the estimation of the scene in line 11.

Algorithm 1 Scene estimation

1: **Input:** Acquired data $\{(\mathbf{a}_i;(\mathbf{y})_i)\}_{i=1}^m$, the maximum number of iterations T, and a low pass filter $\mathcal{G}$.
2: $\tilde{\mathbf{z}}^{(0)} \leftarrow$ Chosen randomly.
3: **Set** $\overline{I}_0$ as the set of indices corresponding to the $|\overline{I}_0|$ largest values of $\{(\mathbf{y})_i/\|\mathbf{a}_i\|_2\}$.
4:
$$(\bar{\mathbf{y}})_i = \begin{cases} 1, & i\in\overline{I}_0 \\ 0, & \text{otherwise} \end{cases}. \tag{11}$$
5: $\mathbf{S} \leftarrow \left[\frac{\mathbf{a}_1}{\|\mathbf{a}_1\|_2},\cdots,\frac{\mathbf{a}_m}{\|\mathbf{a}_m\|_2}\right]^H$.
6: **for** $t=0:T-1$ **do**
7: Compute $\bar{\mathbf{z}}^{(t+1)} \leftarrow \mathbf{S}^H\left(\bar{\mathbf{y}}\circ\mathbf{S}\tilde{\mathbf{z}}^{(t)}\right)$.
8: Compute $\bar{\mathbf{z}}^{(t+1)} \leftarrow \mathcal{G}\left(\bar{\mathbf{z}}^{(t+1)}\right)$. ▷ Filtering step
9: Update $\tilde{\mathbf{z}}^{(t+1)} \leftarrow \frac{\bar{\mathbf{z}}^{(t+1)}}{\left\|\bar{\mathbf{z}}^{(t+1)}\right\|_2}$.
end for
10: Compute $\mathbf{z}_0 = \sqrt{\frac{\sum_{i=1}^m (\mathbf{y})_i}{m}}\tilde{\mathbf{z}}^{(T)}$. ▷ Scaling step
11: **Return:** $\mathbf{z}_0$

B. Target Detection Procedure

This section describes a target identification procedure that follows a template matching strategy using a circular harmonic filter (CHF) [5]. We choose this type of filter because it is invariant to rotations [6]. Specifically, the detection step is divided into two stages: (i) correlation analysis step based on CHF, and (ii) decision step considering a thresholding procedure.

1) Correlation Analysis: A circular filter using a reference pattern has to be designed to detect a target through correlation analysis. Correlation analysis is a metric commonly used in TM, which calculates the similarity between a CHF and a scene. Mathematically, the CHF based on a reference pattern $\mathbf{G}$ of an object in the Fourier domain [15], can be expressed as $\mathbf{H}(\rho,\phi)=\mathbf{b}(\rho)\circ e^{2j\boldsymbol{\theta}}$ where

$$\mathbf{b}(\rho) = \sum_{l=1}^{n} \frac{\mathbf{B}(\rho,(l-1)\Delta\phi)}{|\mathbf{B}(\rho,(l-1)\Delta\phi)|} e^{-2j(l-1)\Delta\phi}, \tag{12}$$

and $\mathbf{B}=\mathcal{F}(\mathbf{G})$. Further, it is worth to mention that matrices $\mathbf{B}$, and $\mathbf{H}$ are initially built in polar coordinates $(\mathbf{r},\boldsymbol{\theta})$.

Now, if we calculate the circular filter $\mathbf{H}(\rho,\phi)$ in rectangular coordinates, denoted by $\mathbf{H}(u,v)$, we have that the correlation matrix $\mathbf{C}$ between the CHF and the reference pattern is given by

$$\mathbf{C}(u,v) = \mathcal{F}^{-1}\left(\overline{\mathbf{H}}(u,v)\circ\mathbf{Z}_0(u,v)\right), \tag{13}$$

where $\mathbf{Z}_0$ is the Fourier transform of the estimated scene obtained from (9).

2) Decision Process: Once the correlation matrix is calculated following (13), we are able to detect a target. More precisely, this target is identified using a threshold, defined as the maximum absolute value of the correlation matrix multiplied by a tolerance parameter. Mathematically, the decision rule for determining a target is given by

$$(\mathbf{R})_{k,l} = \begin{cases} 1, & \text{if } |(\mathbf{C})_{k,l}| \geq \varepsilon\cdot\max(\mathbf{C}) \\ 0, & \text{otherwise} \end{cases}, \tag{14}$$

where $(\mathbf{R})_{k,l}\in\{0,1\}$ represents the elements of the decision matrix, $\varepsilon\in(0,1]$ is a tolerance parameter and $\max(\cdot)$ is an operator that returns an element with the largest magnitude value. In particular, the object of interest is located at an entry (k,l) if $(\mathbf{R})_{k,l}=1$.

Algorithm 2 Target identification

1: **Input:** Acquired data $\{(\mathbf{a}_i;(\mathbf{y})_i)\}_{i=1}^m$, and the tolerance $\epsilon>0$.
2: $\mathbf{z}_0 \leftarrow$Algorithm 1$(\mathbf{a}_i;\mathbf{y})$. ▷ Estimated scene
3: $\mathbf{H} \leftarrow$ Creates the circular filter.
4: Compute $\mathbf{Z}_0=\mathcal{F}\{\mathbf{z}_0\}$.
5: Compute $\mathbf{C}=\mathcal{F}^{-1}\{\overline{\mathbf{H}}\circ\mathbf{Z}_0\}$. ▷ Correlation step
6: $\mathbf{R} \leftarrow$ Builds the decision matrix. ▷ See (14)
7: **Return:** $\mathbf{R}$

Algorithm 2 summarizes the proposed target identification procedure. Note that Algorithm 2 requires the acquired CPD and the tolerance $\epsilon>0$. Then, in line 2 the estimation of the scene is evaluated from the phaseless measurements by Algorithm 1. Further, in line 3 the circular filter is designed from a reference pattern. The Fourier transform of the estimated scene is calculated in line 4. In line 5, the correlation matrix is computed using (13). In line 6, a target is detected using the decision matrix described in Eq (14). Finally, the decision matrix is returned in line 7. The computational complexity of the detection procedure is $\mathcal{O}(n\log(n))$ according to the computed correlation in the Fourier domain.

IV. Simulations and Results

In this section, the performance evaluation of the proposed target identification methodology is presented, under noisy scenarios. Specifically, we test our methodology for different values of signal-to-noise ratio (SNR), which is defined as $\mathrm{SNR} = 20\log(\|\mathbf{y}_\ell\|_2/\|\boldsymbol{\sigma}\|_2)$, with $\boldsymbol{\sigma}$ as the variance of the noise. All the experiments are performed varying noise levels as $\mathrm{SNR} \in \{5, 10, 20, 30\}[\mathrm{dB}]$ and number of snapshots as $L \in \{1, 2, 3, 4, 5, 6, 7, 8\}$. Numerical tests are performed to determine the success rate according to correct identification. This metric is defined as the number of favorable outcomes divided into the total number of possible outcomes. Moreover, the accuracy of the resulting estimation using the proposed initialization is analyzed by calculating the relative error between the original scene and its estimation. The relative error is defined as $\mathrm{dist}(\mathbf{w}, \mathbf{x})/\|\mathbf{x}\|_2$.

Furthermore, the discrete random variable d, that we used for all the experiments to build the set of coded apertures is given by $d = \{j, -j, 1, -1\}$. Notice that d trivially satisfies the assumption over the set of coded apertures required in Theorem 1. All the experiments are performed over the magnitude and phase of three different objects, as shown in Fig. 2. These scenes were acquired using a structured light testbed that allows the optical phase estimation of the object.

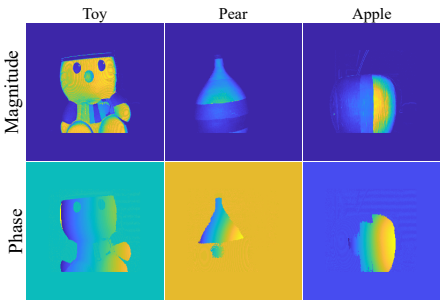

Fig. 2: Magnitude and phase of three different objects acquired through a structured light testbed.

A. Scene Estimation Results

Here, we compare the performance of the proposed initialization via Algorithm 1 with maximum number of iterations $T = 200$ against some traditional initializations such as orthogonality-promoting initialization (OPI) [10], weighted maximal correlation initialization (WMCI) [11] and truncated spectral initialization (TSI) [12]. Specifically, Fig. 3 presents a comparison of the relative error, we take an average of 100 runs of the estimated scenes obtained from the proposed and traditional initializations, for different noise levels, and number of snapshots. Note that the proposed estimation presents the lowest relative error compared to the traditional estimations for all the number of snapshots and noise levels. The proposed initialization is able to appropriately estimate a scene using a single snapshot $L = 1$, while OPI, WMCI and TSI approaches require at least $L = 7$, $L = 4$ and $L = 7$, respectively, to estimate a scene.

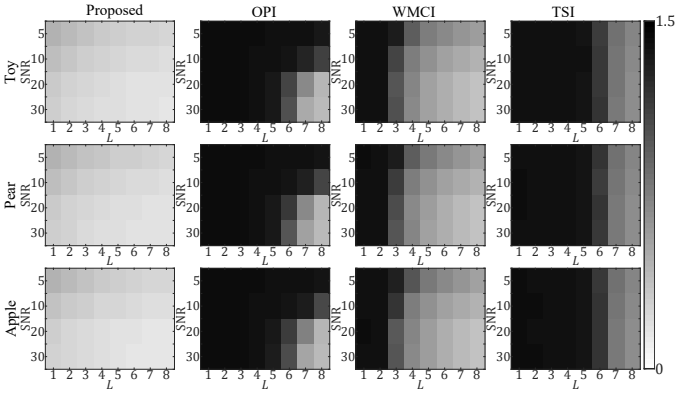

Fig. 3: Summary of the relative error using different initialization strategies, noise levels, and number of snapshots.

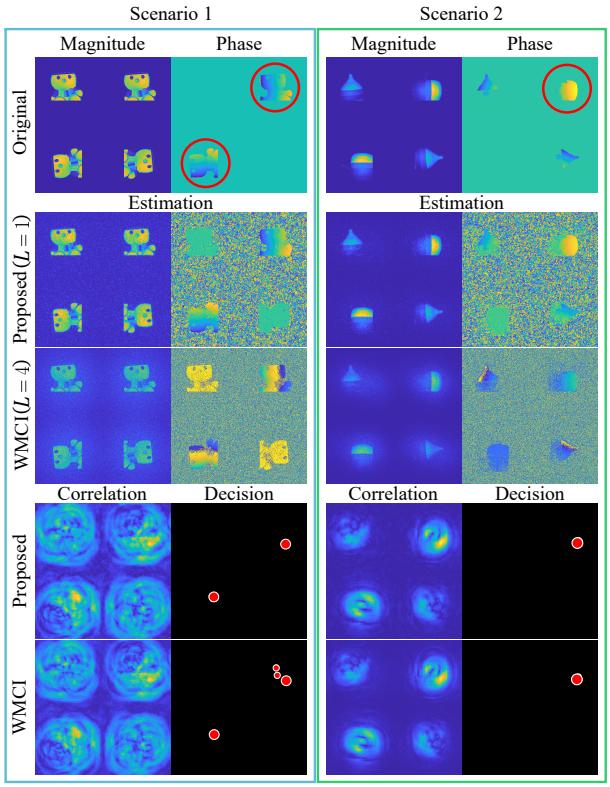

Fig. 4: Target identification methodology using the proposed estimation and WMCI approach with number of snapshots $L = 1$ and $L = 4$, respectively, for two different scenarios with $\mathrm{SNR} = 30[\mathrm{dB}]$.

B. Target Identification Results

In this section, we evaluate the ability of the proposed methodology to correctly detect a target via Algorithm 2 with tolerance $\epsilon = 0.9$. To do that, we test our approach under two different scenarios, as illustrated in Fig. 4. Specifically, the first scenario is composed of four objects (toy objects) with the same magnitude information, with two of them containing non-constant phase information. The second scenario contains four objects (two pear objects and two apple objects), with three of them containing non-constant phase information. In particular, in the first and second scenarios, we are interested in identifying the toy object, and the apple object with phase

information, respectively, which are inside highlighted circles as illustrated in Fig. 4. Notice that from the results shown in Fig. 4, it can be concluded that the identification methodology is able to detect a target using the proposed estimation from a single snapshot, while the proposed identification methodology using WMCI approach requires at least four snapshots to correctly detect the target. The high-intensity zones in the correlation matrix suggest the presence of the target, then, the decision is computed using a thresholding approach over the correlation matrix as (14).

Finally, Fig. 5 displays the success rate using different estimations for the proposed target identification method. In these experiments, we assume that the measurements are corrupted by white noise. Specifically, we test our methodology under different noise levels and different number of snapshots. Observe that these numerical results suggest that a single snapshot is enough to identify a target with a success rate of up to 84% using the proposed estimation method, even when the noise level increases.

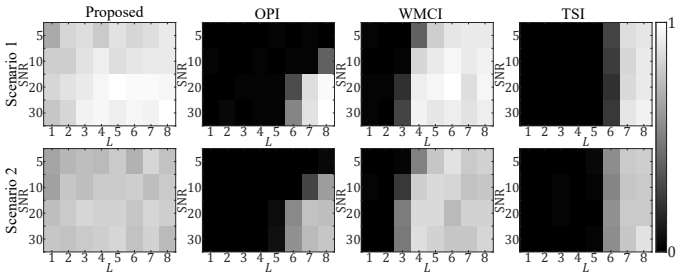

Fig. 5: Summary of the success rate according to the correctly target identification using the proposed methodology by different initializations with different noise levels and number of snapshots.

V. Conclusions

A target identification methodology based on TM from CDP was presented. This methodology is composed of two stages: first, an estimation of the scene is accomplished through a proposed initialization procedure, second, a scanning operation with a reference pattern over the estimated scene is performed using matrix correlation analysis. Further, this methodology uses the optical phase information of an object as an identification discriminant for target detection tasks. Simulation results show that the proposed detection methodology is able to identify a target using one single snapshot with a success rate of up to 84%, even in highly noisy scenarios. In fact, from the numerical tests, it can be concluded that the proposed initialization method requires less number of measurements to better estimate the scene than state-of-the-art initialization approaches.

Acknowledgment

The authors gratefully acknowledge the Vicerrectoría de Investigación y Extensión of Universidad Industrial de Santander for supporting this work registered under the VIE 2467 code, entitled "Optimización de aperturas codificadas para la reconstrucción de patrones de difracción de alta resolución en cristalografía de rayos X, utilizando técnicas de superresolución de imágenes".

Appendix A
Proof of Theorem 1

In this section, we give a brief description of the proof because of limited space. However, for an interested reader, the complete proof can be found in [16]. Then, assuming that

$$\frac{1}{2}\|\mathbf{x}\mathbf{x}^H - \mathbf{z}_0\mathbf{z}_0^H\|_F^2 \leq \frac{\|\mathbf{S}\mathbf{u}\|_2^2}{\|\mathbf{S}\mathbf{x}\|_2^2} \leq \frac{0.99|\overline{I}_0|^2c^2}{4n^4} := \kappa < 1, \tag{15}$$

holds true, where $\mathbf{S} = \left[\frac{\mathbf{a}_1}{\|\mathbf{a}_1\|}, \cdots, \frac{\mathbf{a}_{|\overline{I}_0|}}{\|\mathbf{a}_{|\overline{I}_0|}\|}\right]^H$, and $\mathbf{u} = -\sin(\theta)\mathbf{z}_0 + \cos(\theta)\mathbf{z}_0^{\perp}$. Then, considering that $\sin^2(\theta) = 1 - \cos^2(\theta) \leq \kappa$, we obtain that

$$\begin{aligned}\text{dist}^2(\mathbf{x}, \mathbf{z}_0) &= \|\mathbf{x}\|_2^2 + \|\mathbf{z}_0\|_2^2 - 2\cos(\theta) \\ &\leq 2(1 - \sqrt{1-\kappa}).\end{aligned} \tag{16}$$

Thus, from (16) we have that $\text{dist}^2(\mathbf{x}, \mathbf{z}_0) < 1$, which concludes the proof.

References

[1] T. Bauer, "Pattern recognition in astronomy," *Sterne und Weltraum*, vol. 31, pp. 774–778, 1992.

[2] B. D. Ripley, *Pattern recognition and neural networks*. Cambridge university press, 2007.

[3] P. Geethanjali, "Pattern recognition and robotics," in *Computer Vision: Concepts, Methodologies, Tools, and Applications*. IGI Global, 2018, pp. 1545–1559.

[4] M.-S. Choi and W.-Y. Kim, "A novel two stage template matching method for rotation and illumination invariance," *Pattern recognition*, vol. 35, no. 1, pp. 119–129, 2002.

[5] G. Prémont and Y. Sheng, "Fast design of circular-harmonic filters using simulated annealing," *Applied optics*, vol. 32, no. 17, pp. 3116–3121, 1993.

[6] J. Rosen and J. Shamir, "Circular harmonic phase filters for efficient rotation-invariant pattern recognition," *Applied optics*, vol. 27, no. 14, pp. 2895–2899, 1988.

[7] E. Díaz, J. Meneses, and H. Arguello, "Hyperspectral+ depth imaging using compressive sensing and structured light," in *3D Image Acquisition and Display: Technology, Perception and Applications*. Optical Society of America, 2018, pp. 3M3G–6.

[8] H. Zhang and Y. Liang, "Reshaped wirtinger flow for solving quadratic system of equations," in *Advances in Neural Information Processing Systems*, 2016, pp. 2622–2630.

[9] S. Pinilla, J. Bacca, and H. Arguello, "Phase retrieval algorithm via nonconvex minimization using a smoothing function," *IEEE Transactions on Signal Processing*, vol. 66, no. 17, pp. 4574–4584, 2018.

[10] G. Wang, G. B. Giannakis, and Y. C. Eldar, "Solving systems of random quadratic equations via truncated amplitude flow," *IEEE Transactions on Information Theory*, vol. 64, no. 2, pp. 773–794, 2018.

[11] G. Wang, G. B. Giannakis, Y. Saad, and J. Chen, "Phase retrieval via reweighted amplitude flow," *IEEE Transactions on Signal Processing*, vol. 66, no. 11, pp. 2818–2833, 2018.

[12] Y. Chen and E. Candes, "Solving random quadratic systems of equations is nearly as easy as solving linear systems," in *Advances in Neural Information Processing Systems*, 2015, pp. 739–747.

[13] E. J. Candes, X. Li, and M. Soltanolkotabi, "Phase retrieval from coded diffraction patterns," *Applied and Computational Harmonic Analysis*, vol. 39, no. 2, pp. 277–299, 2015.

[14] Z. Wei, W. Chen, and X. Chen, "Frequency subspace amplitude flow for phase retrieval," *JOSA A*, vol. 35, no. 6, pp. 1074–1080, 2018.

[15] O. Gualdron and H. H. Arsenault, "Phase derived circular harmonic filter," *Optics communications*, vol. 104, no. 1-3, pp. 32–34, 1993.

[16] "Supplementary material," http://diffraction.uis.edu.co/pdfs/AJ.pdf, accessed: 2019-02-28.